SUPPLEMENTARY INFORMATION

Supplementary Tables

3M4CA	2YYWA	3OA8A	2B7SA	1SP3A	1FGJA	2J7AA	3M15A
1S05A	2YYXA	2C1DA	1M64A	1SP3A	1FGJA	2J7AC	1M1QA
1CGOA	2J8WA	2C1DA	2E84A	1SP3A	1QO8A	1KSUA	3BNJA
1CGNA	2ZZS1	1CZJA	2E84A	1GU2A	1Q9IA	1KSSA	1W7OA
2RDZA	1GYOA	1EYSC	2E84A	2XLWA	2DVHA	2BQ4A	2VR0A
2OT4A	2XM4A	1EYSC	2E84A	2XLEA	1GQAA	2BQ4A	1VRNC
1J0PA	1OFWA	3PMQA	2E84A	2XL8A	2CCYA	1FT5A	1MDVA
1J0OA	1OFWA	1AQEA	2E84A	2XL6A	1MQVA	1FT5A	1H32A
1H29A	1WADA	3L1MA	1P2HA	2XLMA	1A7VA	1LJ1A	1H32A
1H29A	2WJNC	2CTHA	1P2EA	1DUWA	1DT1A	2CDVA	3H34A
1H29A	2WJNC	2CY3A	2BC5A	1DUWA	1Y0PA	3HNKA	
1H29A	1BBHA	3CYRA	2YXCA	3FOOA	1Z1NX	3HNJA	
1H29A	1CPQA	1D4DA	3H4NA	3FO3A	1Z1NX	1JRXA	
1H29A	1CPRA	1D4CA	2A3MA	1QDBA	1Z1NX	1JRYA	
1H21A	1I77A	3QW0A	2CVCA	2EWKA	1Z1NX	1JRZA	
2P0BA	3ML1B	1WR5A	2CVCA	2EWIA	1Z1NX	19HCA	
2JBLC	1E39A	1C52A	2CVCA	2EWUA	1Z1NX	19HCA	
2JBLC	3DE8A	3C62A	2CVCA	2Z47A	1Z1NX	1FS7A	
3IQ5A	3CAOA	3C63A	2CVCA	3NMIA	3RKHA	1FS9A	
2RF7A	1OAHA	2B7RA	2CVCA	1FGJA	1UP9A	3SCEA	

Table S1. PDB codes of *c*-type cytochromes with heme C binding sites located on a helix. Multiple entries for single PDB ID's indicate multiple helix-bound *c*-type heme sites are located within a single protein.

	Oxyferrous λ_{max} (nm)			
c-type cytochromes	***γ***	***β***	***α***	***Ref***
2	**410**	**535**	**571**	**This work**
Iso-1-cytochrome *c* M80A	408	537	570	30
Semi-synthetic horse heart cytochrome *c* M80A	n/a	535	571	31
SHP (*Sphaeroides* heme protein)	408	538	570	32

Table S2. UV/visible absorbance data for *c*-type cytochrome oxyferrous species, comparing the maquette, **2,** with methionine-to-alanine mutants of cytochrome *c* and wild type SHP (*Sphaeroides* heme protein).

Heme protein	k_{auto} (h^{-1})	$t_{1/2}$ (s)	*Temp* (°C)	*Ligation*	*Heme*	*Ref*
2	**165**	**15**	**15**	**His/His***	***c*-type**	**This work**
1.5	240	10	15	His/His*	*b*-type	This work
1	266	9.4	15	His/His*	*b*-type	This work
Murine neuroglobin	19	130	37	His/His*	*b*-type	33
Human neuroglobin	5.4	460	37	His/His*	*b*-type	33
Sperm whale myoglobin	0.083	3×10^4	35	His	*b*-type	34
P450cam - camphor	51	50	25	Cys	*b*-type	37
P450 3A4 + testosterone	1300	1.9	4	Cys	*b*-type	38
P450 BM3 + arachidonic acid	792	3.15	20	Cys	*b*-type	39
Iso-1 cytochrome *c* M80A	0.01	2×10^5	22	His	*c*-type	35
SHP	14	180	25	His	*c*-type	36

Table S3. Comparison of oxyferrous state autoxidation rates (k_{auto}) and half lives ($t_{1/2}$) of the maquette, **2**, with natural oxygen binding proteins. Though less stable to autoxidation with respect to the globins, **2** exhibits autoxidation kinetics in the range of the oxygen binding and activating cytochromes P450. Ligation refers to the iron-coordinating ligands in the ferrous heme state. * - The neuroglobins and oxygen binding maquettes undergo rapid ligand exchange at the distal histidine site, and the heme ligation can be considered as an equilibrium between 6-coordinate bis-histidine and 5-coordinate mono-histidine states.

Supplementary Figures

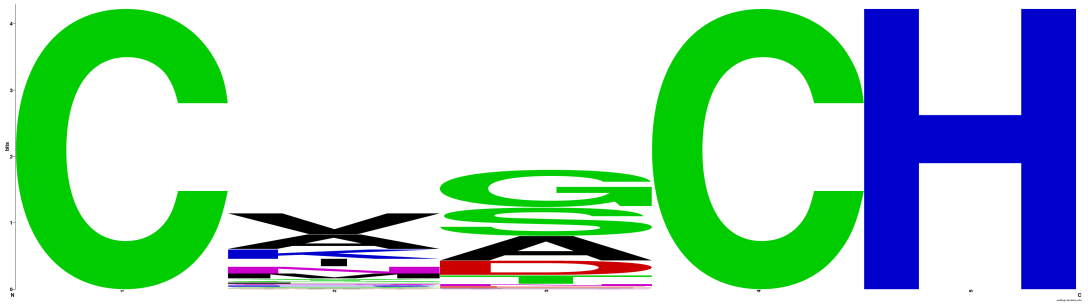

Fig. S1. Weblogo of 150 helical *c*-type heme CX_1X_2CH motifs extracted from the Protein Data Bank (PDB, http://www.rcsb.org/pdb/home/home.do). PDB files of natural cytochromes were downloaded from the non-redundant structural database (from the PISCES server) where the following conditions were satisfied: any CXXCH motif found on a helix of a non-redundant structure containing HEM or HEC. PDB files were hand-curated, the *c*-type binding motif recorded then visualized using WebLogo. A full list of downloaded PDB files can be found in **Table S1**.

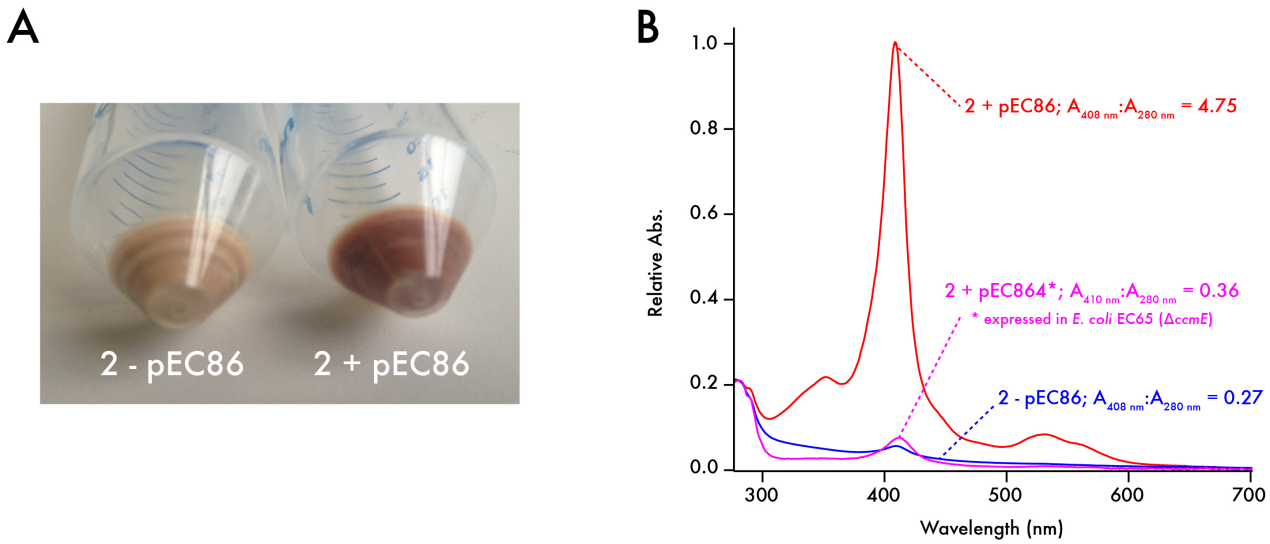

Fig. S2. Covalent heme incorporation is dependent on the presence of the heme lyase CcmE. **A,** The harvested pellet of *E. coli* expressing **2** in the absence (left) and presence (right) of the *ccmA-H* containing pEC86 vector indicates a significant increase in heme concentration *in vivo* when the vector is present. **B,** UV/visible spectroscopic comparison of Ni-sepharose purified **2** expressed in the absence (blue) and presence (red) of the pEC86 vector harboring the fully functional *c*-type cytochrome maturation apparatus. When co-expressed in *E. coli* strain EC65 (Δ*ccmE*) with pEC864 – a variant of pEC86 with catalytically inactive CcmE (H130A CcmE) – no *c*-type heme is observed and the protein instead is purified with *b*-type heme bound (magenta). All traces are normalized to the protein absorbance at 280 nm, and ratios of the absorbances at 408:280 nm (for *c*-type heme) or 410:280 nm (for *b*-type heme) to compare levels of heme incorporation.

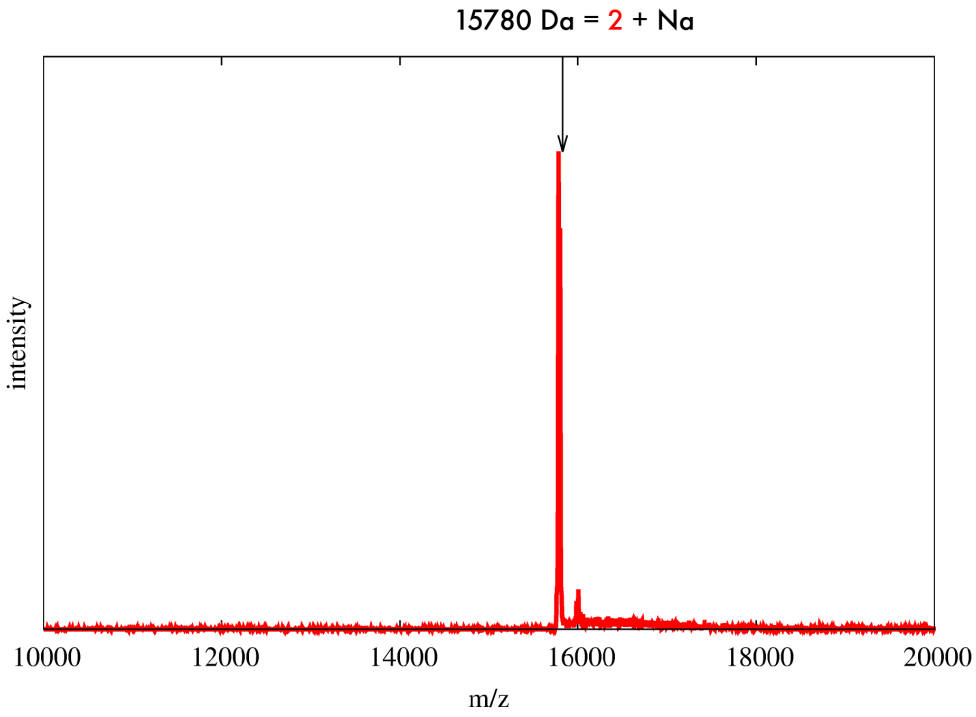

Fig. S3. MALDI-TOF mass spectrum of **2** (MW = 15758 Da) collected on a 4700 TofTof mass spectrometer (Applied Biosystems).

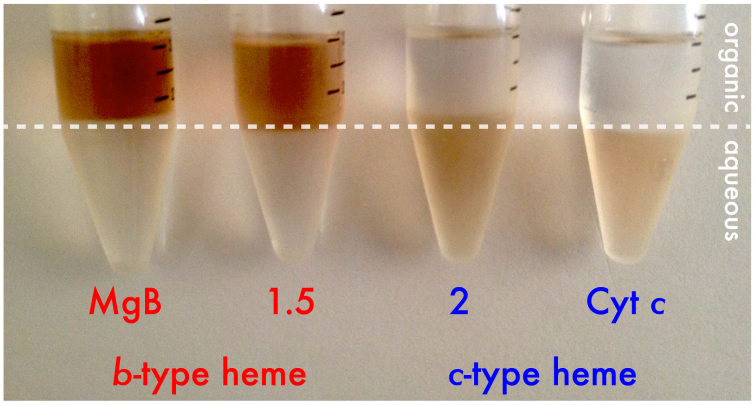

Fig. S4. The *c*-type heme-containing cytochrome *c* (Cyt *c*) and **2** retain heme and remain in the aqueous buffer-containing layer following treatment with acidified 2-butanone (2 ml of protein at 50 μM, 20 mM phosphate, 100 mM KCl, pH 7.5 added to 2 ml acidified 2-butanone at -10 ^{o}C, stirred for 5 minutes then allowed to partition) indicating covalent attachment of the heme to the protein backbone, while the *b*-type heme-containing myoglobin (MgB) and **1.5** experience heme loss to the organic layer due to cleavage of the histidine-heme linkages.

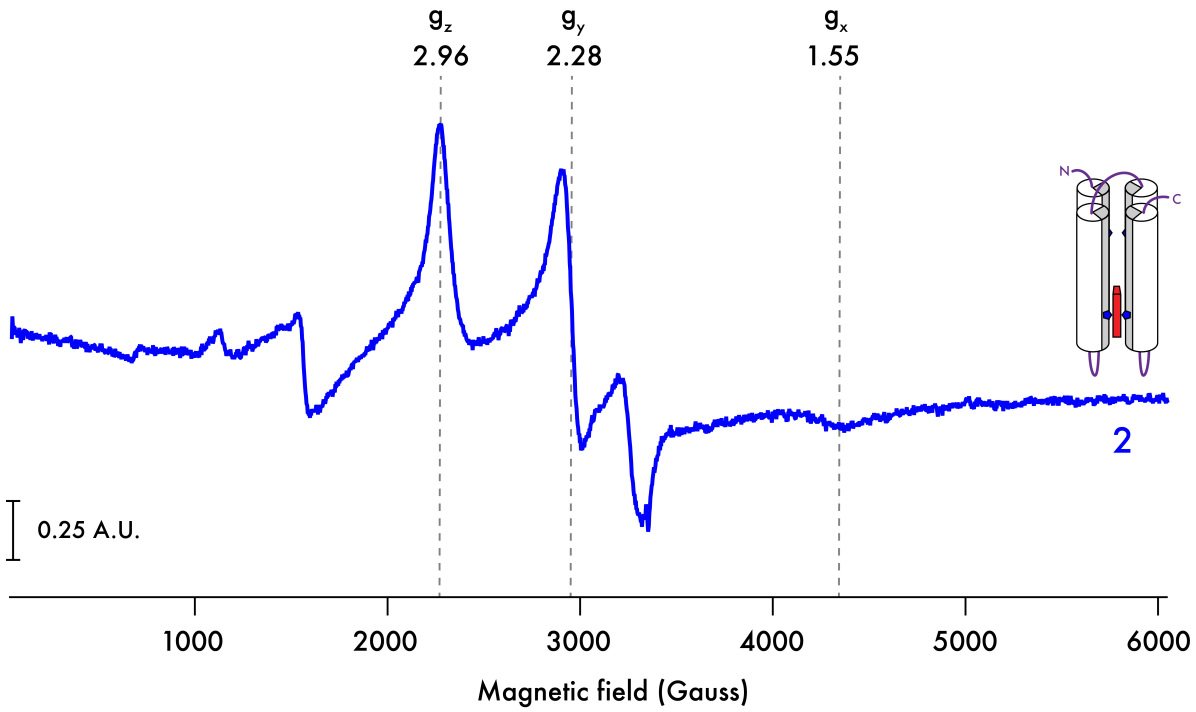

Fig. S5. EPR spectrum of ferric **2** (50 μM protein in 20 mM phosphate, 100 mM KCl), recorded at 10 K, 2 mW power.

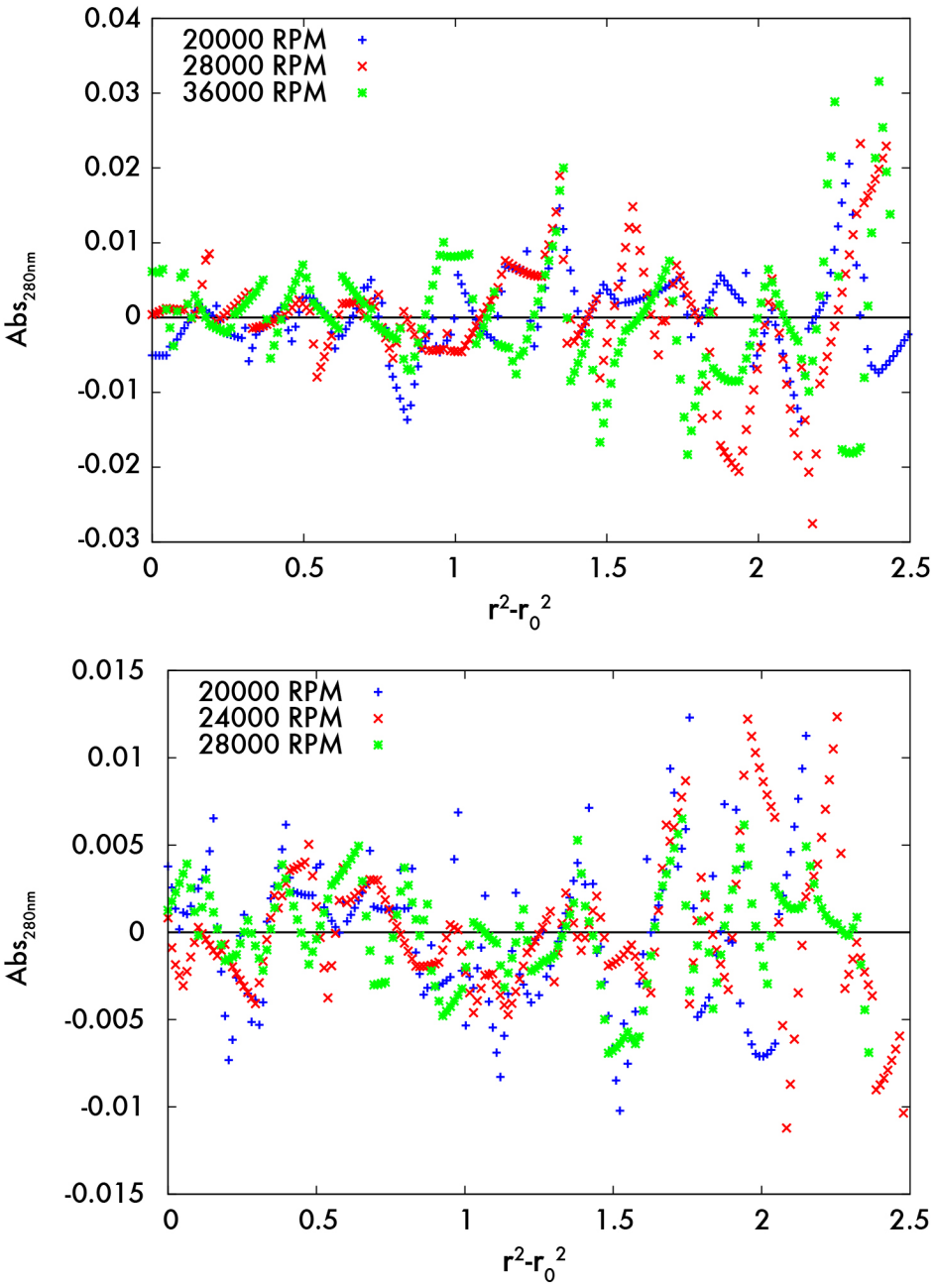

Fig. S6. Residuals calculated from the fitted Analytical Ultracentrifugation data. **Upper panel** - **2**; **Lower panel** - **2** + Heme B.

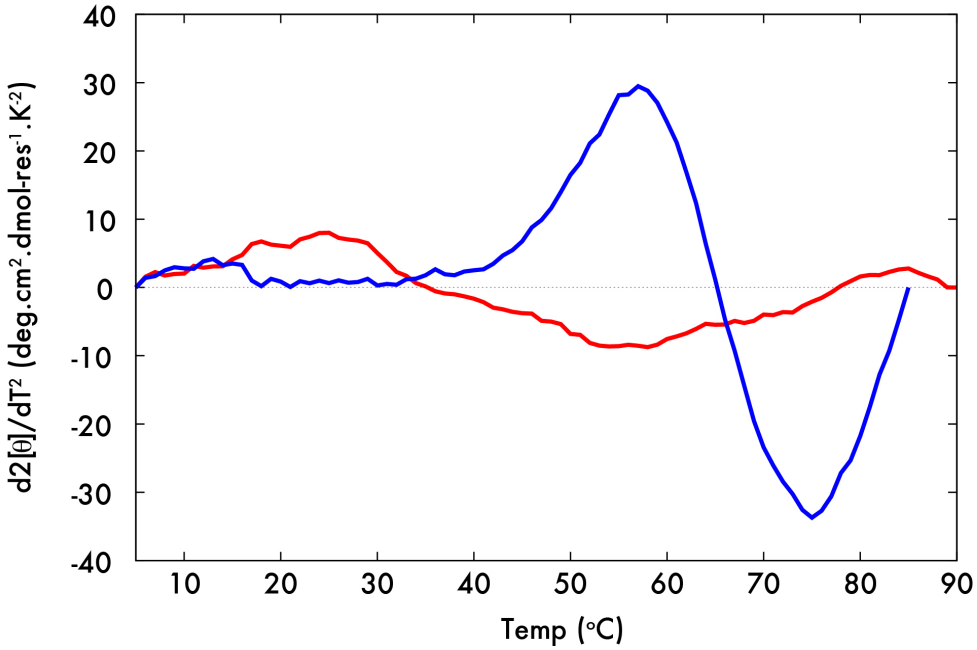

Fig. S7. Second derivatives of the CD melt data for **2** (red) and **2** + heme B (blue) indicating melting temperatures of 34 °C and 66 °C respectively. Experimental conditions as described in **Fig. 6**.

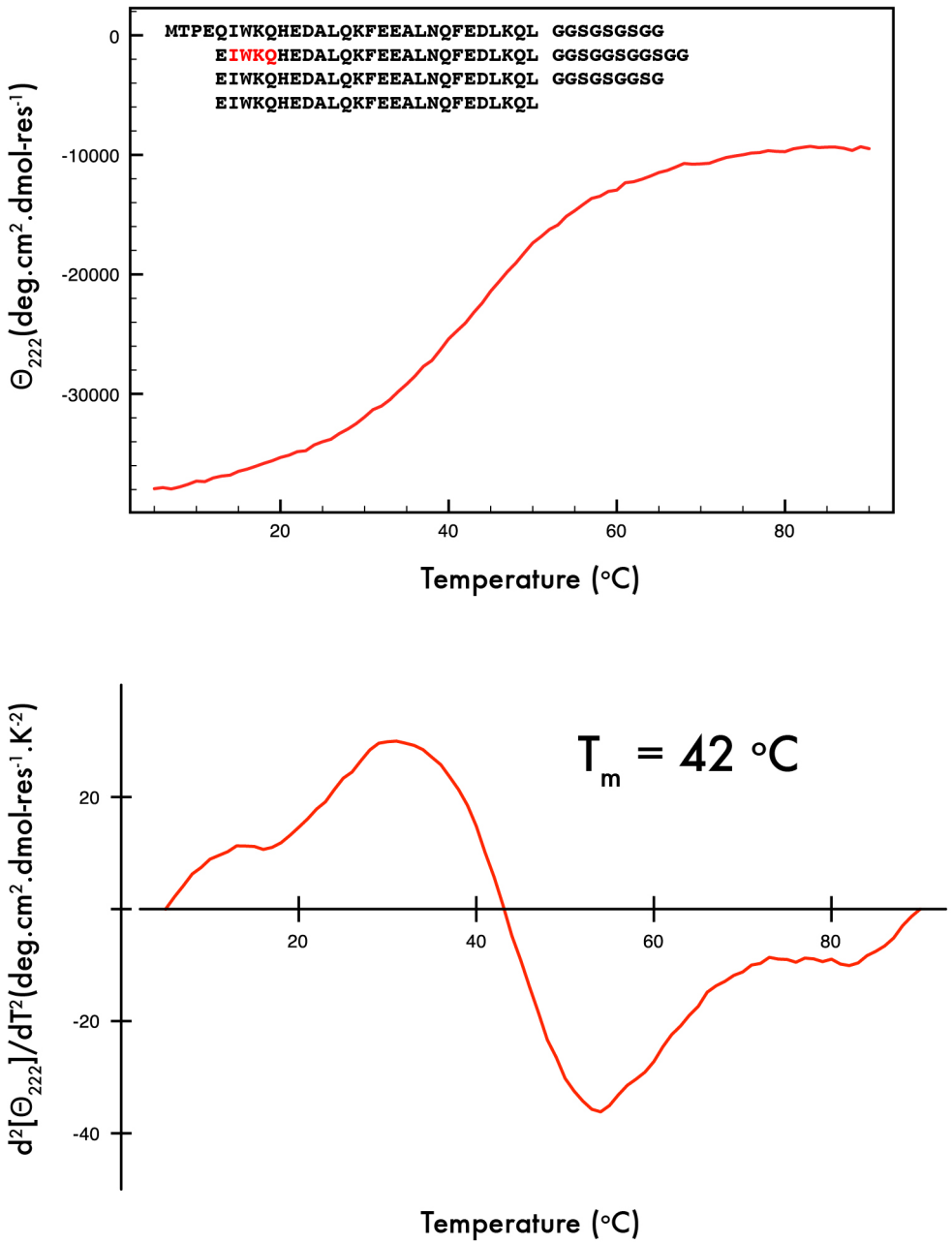

Fig. S8. Temperature dependence of the CD signal @ 222 nm for apo-**1.5** (upper panel) – the single chain maquette lacking the CXXCH motif - and the second derivative of the temperature dependence data (lower panel, Apo-**1.5**, T_m = 42 ^{o}C). The amino acid sequence of 1.5 is displayed in the upper panel. Differences with respect to **2** are highlighted in red.

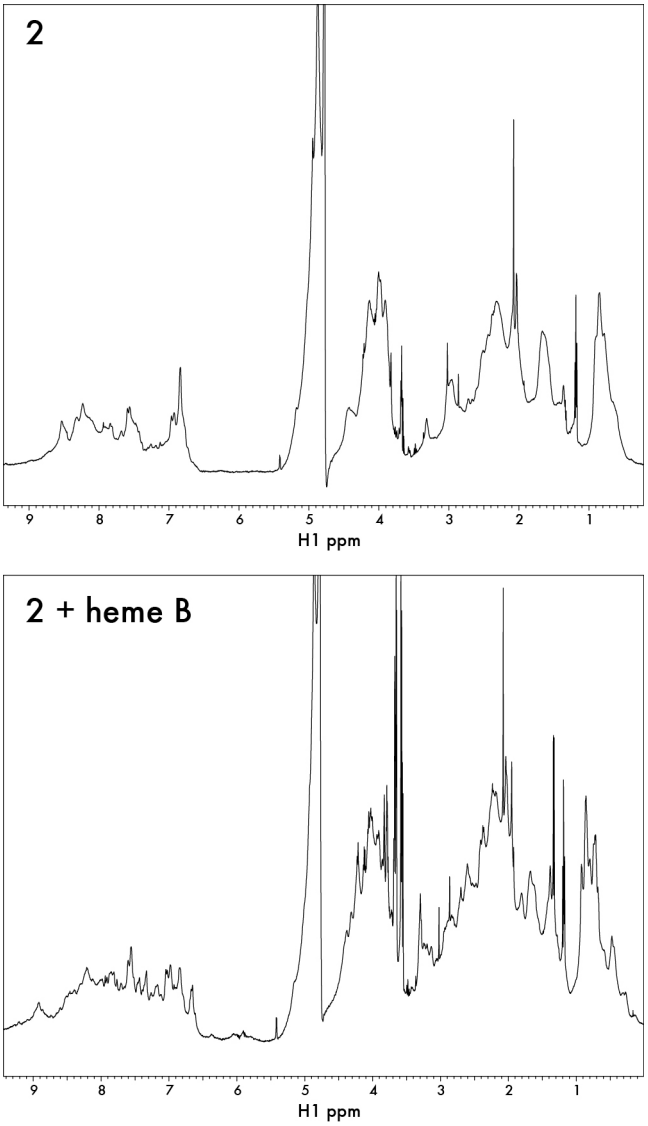

Fig. S9. Heme B-mediated structuring of **2**. ^{1}H NMR spectra of **2** (upper panel) and **2** + heme B (lower panel). Spectra recorded on a Varian INOVA 600 MHz spectrometer at 500 µM **2** in redox buffer containing 10 % v/v D_2O.

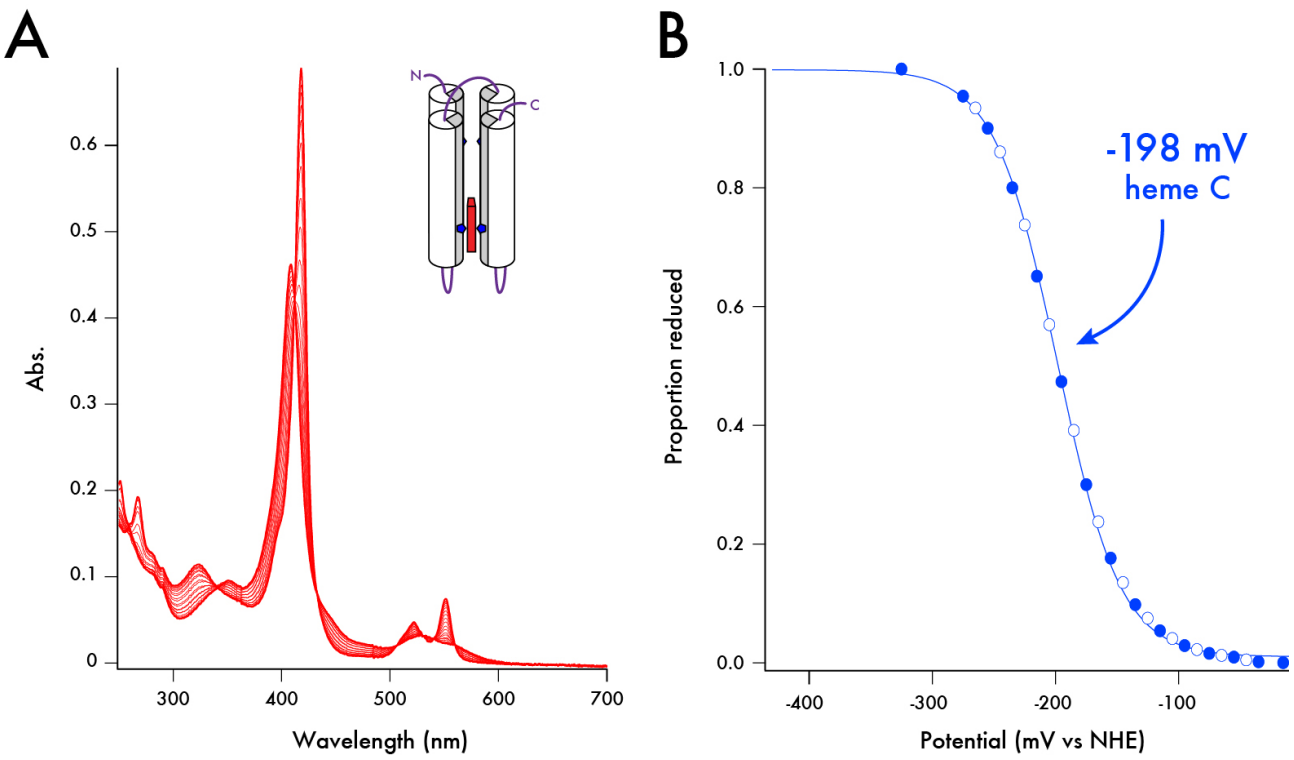

Fig. S10. Redox potential of heme C in **2. A.** UV/visible spectra of potentiometric titrations of **2** (130 µM, 50 mM phosphate, 500 mM KCl, 10% glycerol, pH 7.5) **B.** Determination of redox potential of *c*-type heme in **2**. Reductive (closed circles) and oxidative (open circles) data are fitted with 1-electron Nernst curves and quoted *vs* the Nernst hydrogen electrode (NHE). The proportion of reduced heme (*y-axis)* was determined at 418 nm.

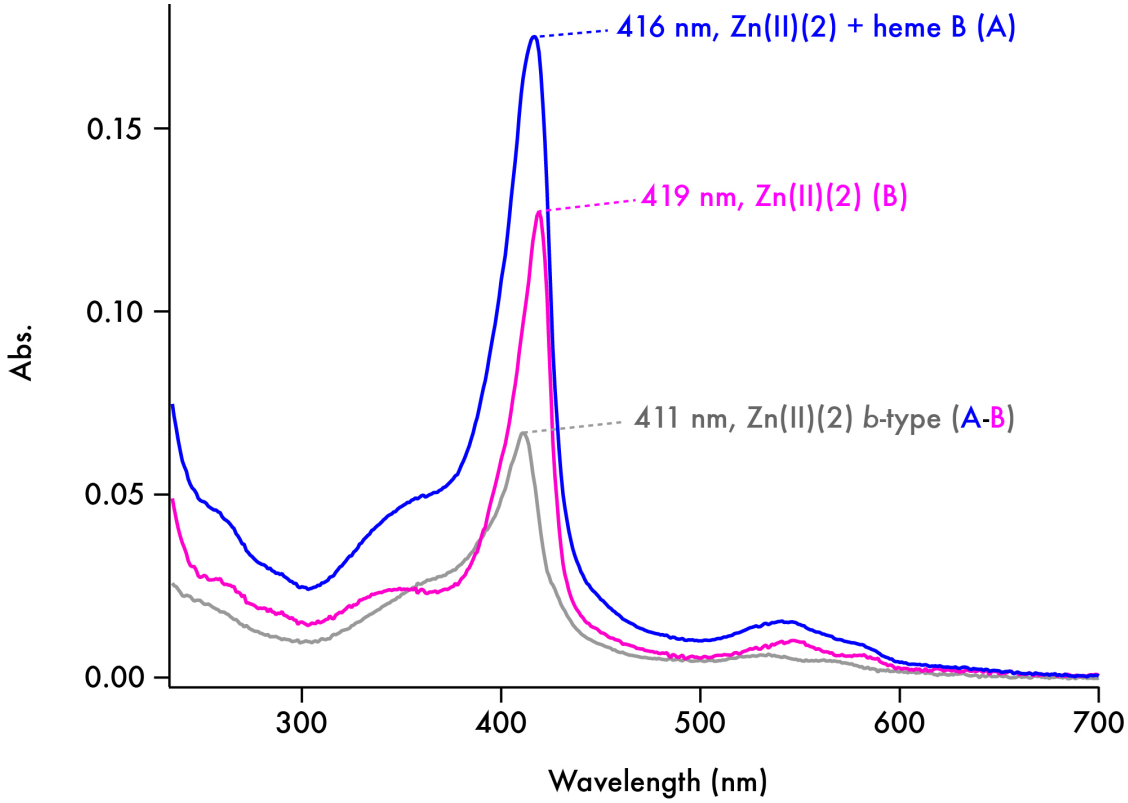

Fig. S11. Formation of a light sensitive porphyrin dyad in **2**. UV/visible spectra of Zn(II)(**2**) and Zn(II)(**2**) + 1 equivalent of heme B (900 nM **2**, 20 mM CHES, 150 mM KCl, pH 9.0). A difference spectrum is displayed, indicating the successful incorporation of a bis-histidine ligated heme B in the available tetrapyrrole binding site.